AIAA-2004-0765
Compressibility and Leading-Edge Bluntness Effects for a 65° Delta Wing

J. M. Luckring
NASA Langley Research Center
Hampton, Virginia

42nd AIAA Aerospace Sciences Meeting & Exhibit
5-8 January 2004
Reno, Nevada

Compressibility and Leading-Edge Bluntness Effects for a 65° Delta Wing

J. M. Luckring*
Aerodynamics, Aerothermodynamics, and Acoustics Competency
NASA Langley Research Center
Hampton, Virginia

ABSTRACT

A 65° delta wing has been tested in the National Transonic Facility (NTF) at mean aerodynamic chord Reynolds numbers from 6 million to 120 million at subsonic and transonic speeds. The configuration incorporated a systematic variation of the leading edge bluntness.

The analysis for this paper is focused on the compressibility and bluntness effects primarily at a Reynolds number of 6 million from this data set. Emphasis is placed upon on the onset and progression of leading-edge vortex separation, and compressibility is shown to promote this separation. Comparisons with recent publications show that compressibility and Reynolds number have opposite effects on blunt leading edge vortex separation

NOMENCLATURE

AR	wing aspect ratio, 1.8652
b_{le}	leading-edge bluntness, r_{le}/c_{bar}
b/2	wing semispan, 1.0 ft.
C_p	pressure coefficient
$C_{p,le}$	leading-edge pressure coefficient
$C_{p,v}$	vacuum pressure coefficient
C_p*	sonic pressure coefficient
c	wing chord
c_{bar}	wing mean aerodynamic chord, 1.4297 ft.
$c_{l,max}$	section maximum lift coefficient
c_r	wing root chord, 2.1445 ft.
c_t	wing tip chord, 0 ft.
d	sting diameter, 0.275 ft.
d/b	nondimensional sting diameter, 0.1375
M	Mach number
Rn	Reynolds number, based on c_{bar}
r_{le}	streamwise leading-edge radius
S	wing reference-area, 2.1445 ft^2
t	wing thickness, 0.875 in.
t/c_{bar}	nondimensional wing thickness, 0.051
w_{ts}	NTF test section width, 8.2 ft.
x,y,z	Body-axis Cartesian coordinates
x_m,z_m	match coordinates, leading-edge contour
x_v	Longitudinal coordinate, vortex separation
α	angle of attack
η	percent semispan location, 2y/b
Λ_{le}	wing leading-edge sweep
λ	wing taper ratio, c_t/c_r, 0.

* Senior Research Engineer, Configuration Aerodynamics Branch, Associate Fellow, AIAA

INTRODUCTION

Separation-induced vortex flows can occur on a wide range of aircraft component scales. In some cases they have been exploited such as with strakes for development of maneuver lift increments, in other cases they have arisen in conjunction with other design considerations such as with forebody and inlet edging for low observability. Fundamental properties of these vortices and their interactions with aircraft components need to be understood for any successful design application, irrespective of whether the vortex is to be exploited, tolerated, or avoided.

Studies of these vortex flows have ranged from fundamental delta wing investigations[1-4] to full aircraft assessments.[5-7] Early research was performed primarily at low speeds and focused on wings with sharp leading edges[1-4] where the primary vortex separation is fixed by this geometric feature. Practical wing designs incorporate blunt leading edges, and this bluntness greatly complicates the aerodynamics of leading-edge vortex flows.

The fundamental complication contributed by the blunt leading edge is illustrated in Figure 1 for a delta wing. In the sharp-edged case, primary vortex separation occurs at the leading edge and the origin of the vortex is at the apex of the delta wing. In the blunt-edged case, the origin of the vortex separation is displaced from the apex of the wing and varies with many flow and geometry properties. For example, at low angles of attack the blunt-edged wing can develop wholly attached flow, and as angle of attack increases the origin of leading-edge vortex separation will progress up the leading edge. The blunt leading

edge wing will support a hybrid of attached flow and leading-edge vortex flow.

A blunt leading edge evokes flow physics that are otherwise suppressed by the sharp leading edge, particularly as regards flow separation. By way of an example, leading edge separation properties for a NACA 0012 airfoil are reviewed in Figure 2. In this figure (from Polhamus[8]) the experimental effects of Mach number and Reynolds number on the section maximum lift coefficient ($c_{l,max}$) are summarized. For these data $c_{l,max}$ is determined from leading-edge separation effects, and the data were taken in a manner to isolate Reynolds number and Mach number effects. The data show an increase in $c_{l,max}$ as Reynolds number is increased due to delayed separation. They also show that $c_{l,max}$ decreases as Mach number increases. Even for the low Mach numbers of the investigation local compressibility (and expected shock-induced separation) near the leading edge result in a trend opposite that of Reynolds number effects. If Reynolds number and Mach number were varied simultaneously (as in a constant pressure tunnel) these effects would be confounded.

The author has recently published two papers to address Reynolds number and bluntness effects on leading-edge vortex separation at subsonic[9] (M=0.4) and transonic[10] (M=0.85) speeds. These analyses are based upon an extensive and unique data set[11-14] obtained in the NASA Langley National Transonic Facility.[15-17] The tests were designed to isolate Reynolds number and Mach number (compressibility) effects on leading-edge vortex separation for a 65° delta wing with various leading-edge bluntness values.

The present investigation is directed at quantifying the effects of compressibility and leading-edge bluntness on the onset and progression of leading-edge vortex separation for a 65° delta wing. Selected results are presented from the same NTF data set mentioned above. The data selected for this analysis were obtained at free-stream Mach numbers of 0.4, 0.6, and 0.85 and at a Reynolds numbers of 6 million based on the wing mean aerodynamic chord. The compressibility analysis presented in this paper will be focused on contrasting data among the three Mach number conditions. A limited comparison between compressibility and Reynolds number effects will also be included. A brief description of the experimental program follows.

EXPERIMENTAL PROGRAM

The delta wing program was one of the original fundamental tests planned for the NTF. It was envisioned that these data would serve as a good initial assessment of leading-edge bluntness and Reynolds number effects on vortex flow aerodynamics, and that subsequent test programs could be launched based upon analysis of these findings. It was also envisioned that these data would be useful for calibrating computational fluid dynamics predictions of these aerodynamics. To help facilitate numerical analysis, the entire wing and near-field sting were developed as fully analytical surfaces, continuous through second derivative and, hence, curvature.

Facility and test conditions

The experimental program was performed in the National Transonic Facility. The NTF can be operated at Mach numbers ranging from 0.1 to 1.2, at total pressures from 1.1 to 8.8 atmospheres, and at total temperatures from around 120° F down to -250° F, the cryogenic temperatures being achieved through the evaporation of injected liquid nitrogen. The three degrees of freedom for controlling the test medium (speed, pressure, and temperature) allow for independent variation among the three primary aerodynamic free-stream variables (Mach number, Reynolds number, and dynamic pressure). In the context of the present investigation, this capability can be exploited to eliminate certain pseudo-Reynolds number effects.[18] The facility test section is 8.2 feet square and approximately 25 feet long. Addition facility details can be found among References 15-17.

The NTF operating envelope, scaled to the delta wing of the present investigation, is shown in Figure 3. Here the facility Reynolds numbers are based upon the delta wing mean aerodynamic chord and represent maximum operating capability. The Mach and Reynolds number extent for the delta wing experimental program is also shown and is well within the maximum facility capability. In addition, a variety of slender vehicle operating conditions are shown along with those for a typical High-Wing Military Transport (C-17). Although the delta wing is a very fundamental shape, the test program was designed to include conditions relevant to aircraft operations. A representative matrix of test conditions is shown in Figure 3b. Not all of these conditions were achieved for every configuration due to resource limitations.

Wind tunnel model

The model was a full-span delta wing mounted on an offset sting to obtain the desired angle of attack range. A photograph of the model along with some additional model details is provided in Figure 4. The offset sting was designed to keep the model on the tunnel centerline for the full angle-of-attack range investigated.

The model was instrumented with 183 static surface orifices that had an internal diameter of 0.010 inches. (See Figure 4b.) The orifice arrangement allowed for fairly good spanwise resolution at five chordwise stations. Pressure orifices were also located directly on the blunt leading edges to help track the onset and progression of leading-edge vortex separation. Pressures were measured remotely with electronically scanned pressure (ESP) modules.

The model was an uncambered flat plate with special consideration given to the leading and trailing edges. The wing was designed for a series of interchangeable leading-edge components and the leading edge contours are shown in Figure 5. They were defined with a NACA-like airfoil polynomial[19] for four values of leading-edge bluntness, r_{le}/c_{bar}, that were 0 (sharp), 0.0005, 0.0015, and 0.0030 in the streamwise direction. These bluntness values were chosen to be relevant to several aircraft that incorporate thin highly swept wings.[9]

The leading-edge contours matched the flat-plate wing over a distance of 15% root chord and were constant spanwise to match the flat-plate central portion of the wing. This leading-edge contour region is also indicated in Figure 4b. The central flat plate portion of the wing was 5.1 percent thick (referenced to the mean aerodynamic chord) and this thickness was closed out over the last 10-percent of the root chord to a sharp trailing edge. The model was polished to an 8-microinch surface finish.

Experimental procedures

Angle of attack was determined from the combination of arc-sector setting and calibrated sting-bending effects. Data were obtained at only two total temperatures, nominally 120^{o} F and -250^{o} F. Total pressure was varied nominally between 1.1 and 5.3 atmospheres to obtain the desired free-stream test conditions.

It was anticipated that the flow would naturally be turbulent over the Reynolds numbers tested, so artificial transition strips were not used. Moreover, there were no clear transition-strip test techniques for these vortex flows.

A number of potential pseudo-Reynolds-number effects were considered and minimized in the design of the experiment. Calculations indicated that aeroelastic deformation would be small due to the low aspect ratio of the wing, the thickness of the wing, and the stiffness of the material. The 8-microinch surface finish was sufficient for the model to be hydraulically smooth over the range of conditions tested. Wind tunnel wall interference was believed to be negligible due to the slotted test section and the relative size of the delta wing to the test section (b/w_{ts} = 0.244). The model support mechanism was designed to keep the model centered in the test section. This essentially eliminated pseudo-angle-of-attack effects associated with the model traversing the test section flow and/or getting too close to the ceiling at high angles of attack.

RESULTS

Compressibility effects for the sharp-edged delta wing will be discussed first. This analysis will be kept brief in order to allow space for the blunt-edged results. Both compressibility and bluntness effects are presented with a view toward addressing the onset and progression of leading-edge vortex separation. Finally, compressibility and Reynolds number effects will be contrasted.

Sharp-edge configuration

Compressibility is first addressed for the sharp-edge case by contrasting results at two dissimilar Mach numbers, M=0.4 and M=0.85. See Figure 6. The comparison is made at a reference angle of attack of 13^{o} and at a reference Reynolds number of 6 million. In Figure 6 the static surface pressure distributions for the two Mach numbers are shown on the left and right sides. In addition, a direct comparison of these pressures at the 60-percent chord station is shown along with pressure data at M=0.6.

Surface pressures for M=0.4 show a classical leading edge vortex type of pattern. A strong primary vortex suction peak is observed along with outboard pressures indicative of turbulent secondary separation. This would be expected at the subject Reynolds number. The aft stations show the (nonconical) drop in peak suction as well as inboard curvature of the peak suction location in association with trailing-edge effects. Pressures at M=0.4 are fully subsonic.

With regard to compressibility effects for a leading-edge vortex flow, many factors can be considered. Linear theory, in conjunction with Smith's conical flow theory[3], can indicate that peak suction pressures would diminish and shift inboard as Mach number increases. Subcritical compressibility effects can be modeled through potential flow theory with nonlinear vortex sheet boundary conditions, and such a formulation has been shown[20] to approach Smith's conical flow theory[3] through a diminution of trailing-edge effects as Mach number is increased. From this perspective, peak suction pressures near the trailing edge could become more negative and shift outboard.

Nonlinear compressibility effects can dominate these theoretical considerations, and the M=0.85 data in Figure 6 evidence a number of these nonlinear effects. The vortex suction peaks at the forward two stations are suppressed (compared to the data at M=0.4) and yet achieve roughly 64-percent of vacuum. Vortex suction pressures generally exceed sonic values thereby indicating a supersonic leading-edge vortex. It is further noted in the inset that the peak suction pressure for M=0.6 is close to sonic conditions. Nonlinear compressibility thus may contribute significantly even at M=0.6. The peak suction pressures highlighted in the inset diminish in magnitude and shift inboard with increasing Mach number at the 60-percent chord station.

Despite these many nonlinear effects, it is noteworthy that the overall C_p footprint of the M=0.85 vortex flow is as similar as it is to the subsonic M=0.4 case. A major consideration here is that the primary perturbation velocities for the slender-wing vortex flow occur in crossflow plane, nominally orthogonal to free-stream velocity.

Blunt-edge configuration

The bulk of the analysis in this section will be restricted to the data taken at a Reynolds number of 6 million. Relative effects of compressibility and Reynolds number will be addressed with regard to separation onset and progression.

Compressibility effects. Comparison between M=0.4 and M=0.6 for the medium bluntness leading edge at an angle of attack of 13^o is presented in Figure 7. Spanwise pressure comparisons at the 60-percent root chord station show that the primary vortex suction peak has shifted inboard and diminished in magnitude for the higher speed case. However, examination of the pressures at the 40-percent station indicates the increase in Mach number has promoted leading-edge vortex separation. That is, for this fixed angle of attack, the leading edge separation is initiating further upstream for the higher-speed condition.

The onset of leading-edge separation can be more clearly inferred from the leading-edge pressure coefficients. For attached flow these pressures will become more negative (at a fixed angle of attack) with distance down the leading edge and a reversal in this trend can indicate the onset of leading-edge separation. Prior analysis[9,10] showed a good correlation of this trend with leading-edge vortex separation as evidenced from the surface pressure distributions.

Leading-edge pressure coefficients are presented in Figure 8 at the reference angle of attack and Reynolds number for free-stream Mach numbers of 0.4, 0.6, and 0.85. At M=0.4, the leading edge pressures indicate that the origin of leading-edge separation occurs somewhere in the vicinity of 30-percent root chord. By M=0.6 this origin has moved upstream to the vicinity of 20-percent root chord. These observations are consistent with the upper surface pressures.

The leading-edge pressures are also an indication of the body-axis leading-edge thrust. These pressures were integrated down the leading edge to obtain a relative assessment of compressibility effects on leading-edge thrust. Results indicate that the M=0.6 data suffer a 35% loss in leading edge thrust with respect to the M=0.4 data; the M=0.85 data suffer a corresponding 46% thrust loss. This loss of thrust is primarily due to the increased leading-edge separation as Mach number increased.

A more accurate estimate of leading-edge separation can be obtained by assessing angle of attack trends for the leading-edge pressure coefficients. An example is shown in Figure 9 for the leading-edge pressure at 50-percent chord station. (The surface pressure coefficients shown on the wing planforms in this figure are the same as those from Figure 8.) The M=0.4 data indicate that separation occurred between 10^o and 11^o at this station. For M=0.6 separation appears to have occurred closer to 9^o at this same station. Also shown on the figure is the attached-flow angle of attack trend expected from thin-wing theory. The coefficients for the theoretical model were simply obtained from a linear least-squares fit to the data at low angles of attack. The attached flow theory models the flow very well up to the angle of attack where the flow separates at this station.

Angle-of-attack trends including higher Mach number data are shown in Figure 10. The higher speed data in the $0.8 < M < 0.9$ range show a more gradual departure from the attached flow trend as separation passes by this station. Other than this attribute, however, the data show a somewhat surprisingly similar overall trend with angle of attack. By considering the sonic pressure coefficient it is noted that at $M = 0.4$ ($C_p^* = -3.7$) the leading-edge separation is wholly subsonic, at $M = 0.6$ ($C_p^* = -1.3$) the leading-edge separation occurs at supersonic conditions with post-separation subsonic flow, and at $M = 0.85$ ($C_p^* = -0.3$) the leading-edge separation is wholly supersonic. On the scale of Figure 10 the higher speed data show fairly smooth compressibility trends, and for the balance of the paper the M=0.85 data will be included in the analysis as representative of trends in the $0.8< M < 0.9$ speed regime.

Either the longitudinal analysis of Figure 8 or the angle-of-attack analysis of Figure 9 provides a means to estimate the onset of leading edge vortex separation. Due to the relative increments in longitudinal pressure tap distribution and in angles of attack, the angle-of-attack approach is preferable for this experiment

Bluntness contributions. Compressibility effects for the leading-edge pressures are presented in Figures 11 and 12 for the three blunt leading edges. Angle of attack trends in Figure 11 show that, for the small leading edge, separation at the mid chord station occurs around 4^o angle of attack. In addition, there are relatively small effects of Mach number for this leading edge at the conditions shown. The large leading edge delays leading-edge separation and also shows a greater effect of Mach number on the separation.

The angle-of-attack analysis of Figure 11 is presented for the mid-chord leading edge pressure. To assess longitudinal effects, the leading-edge pressure distribution is presented in Figure 12 at 13^o angle of attack. The data show Mach number trends for the entire leading edge that are consistent to those just discussed. Relative to the medium leading edge, the small leading edge shows small compressibility effects whereas the large leading edge shows increased compressibility effects.

To more directly see leading-edge bluntness effects the angle of attack data from Figure 11 are cross-plotted in Figure 13. Here data for the three bluntness values are directly compared for the three Mach numbers being analyzed. The low angle-of-attack attached-flow portion of these comparisons shows the decreased flow acceleration trend for the blunter leading edges with angle of attack that would be expected. At M=0.4 leading-edge bluntness continually extends the angle of attack range for attached flow, and the pressures are essentially all subsonic. At M=0.6 the large bluntness now only provides marginal improvement over the medium leading edge for sustaining attached flow; both of these leading edges develop supersonic flow prior to separation at the station shown. At M=0.85 there are much smaller effects of the leading-edge bluntness as regards sustenance of attached flow. The majority of the data shown at M=0.85 correspond to supersonic flow.

Separation onset and progression. Angle-of-attack analysis of leading-edge pressures has been performed to estimate the onset and progression of blunt leading-edge vortex separation. Results are first presented in Figure 14 for the medium leading-edge case and for the three Mach numbers under consideration. The results distinctly show that an increase in Mach number promotes the onset of leading-edge vortex separation. For example, at M=0.4 the flow stays attached up to approximately 10^o after which the origin of the leading-edge vortex separation move upstream to approximately the mid chord station ($x_v/c_r = 0.5$). Corresponding data for M=0.6 show that this separation onset occurs about two degrees lower in angle attack. At M=0.85 the angle of attack for separation onset is further reduced. The progression of separation up the leading edge is fairly similar among the three Mach numbers shown

The same analysis is presented in Figure 15 for the three blunt leading edges. Once again, the smallest leading edge shows relatively little effect of Mach number whereas the large leading edge shows increased Mach effects as compared to the medium leading edge. An increase in leading edge bluntness also delays the onset and progression of the leading-edge vortex separation.

Previous work[9,10] has addressed the effect of Reynolds number on the onset and progression of leading-edge vortex separation from this same data set. Figure 16 presents Reynolds number effects on blunt leading-edge separation for the medium leading-edge radius at M=0.4 and 13^o angle of attack. The results (from Reference 9) demonstrate the delay in leading-edge separation due to the increase in Reynolds number from a nominal wind tunnel value (6 million) to a representative flight value (60 million).

A comparison of compressibility effects from the present study to Reynolds number effects[9] for the subject leading-edge separation is presented in Figure 17. The baseline conditions for this Figure are M=0.4 and a Reynolds number of 6 million. As shown previously, this increase of Mach number (at constant Reynolds number) from 0.4 to 0.6 promotes leading edge separation. The increase of Reynolds number (at constant Mach number) from 6 million to 60 million delays the leading-edge separation. The effects of Mach number and Reynolds number are opposite in sign and comparable in magnitude for this case. Thus, it seems to be very important to isolate these effects from one another for modeling or prediction purposes.

FINAL REMARKS

An analysis of compressibility and leading-edge bluntness effects for the flow about a 65° delta wing has been presented. Analysis was focused upon data obtained at free-stream Mach numbers of 0.4, 0.6, and 0.85 out of an extensive data set generated in the NTF. Compressibility effects were analyzed at a constant Reynolds number of 6 million.

A limited analysis of data for the sharp-edged delta wing indicated that the primary vortex suction peak was suppressed (less negative) at the higher Mach numbers. At M=0.6 the surface flow induced by the primary vortex was already reaching sonic conditions, and by M=0.85 the flow induced by the leading-edge vortex is locally supersonic over much of the wing upper surface.

For the blunt leading edge configurations compressibility was shown to promote leading-edge vortex separation, and significant differences between the M=0.4 and the M=0.6 data were found in association with compressibility effects. Beneficial bluntness effects for sustaining attached flow at low speeds were curtailed at the higher speeds.

Finally, Mach number and Reynolds number were shown to have opposite effects for the onset and progression of leading-edge vortex separation. Compressibility promotes this separation whereas Reynolds number postpones it. Although opposite in sign, these effects can be comparable in magnitude. It seems crucial therefore to be able to isolate these effects in order to physically understand, model, and predict blunt leading edge separation on slender wings.

REFERENCES

[1]Polhamus, E. C., "A Concept of the Vortex Lift of Sharp-Edged Delta Wings Based on a Leading-Edge Suction Analogy," NASA TN D-3767, 1966.

[2]Hummel, D., "On the Vortex Formation Over a Slender Wing at Large Incidence," AGARD CP-247, Paper No. 15, January 1979.

[3]Smith, J. H. B., "Improved Calculations of Leading-Edge Separation from Slender Delta Wings". RAE TR-66070, 1966.

[4]Hemsch, M. J., and Luckring, J. M., "Connection Between Leading-Edge Sweep, Vortex Lift, and Vortex Strength for Delta Wings," AIAA J. Aircraft, Vol. 27, No. 5, May 1990.

[5]"High Angle of Attack Aerodynamics," AGARD CP-247, January 1979.

[6]"Aerodynamics of Vortical Type Flows in Three Dimensions," AGARD CP-342, July 1983.

[7]"Vortex Flow Aerodynamics," AGARD CP-494, July 1991.

[8]Polhamus, E. C., "A Survey of Reynolds Number and Wing Geometry Effects on Lift Characteristics in the Low Speed Stall Region," NASA CR-4745, 1996.

[9]Luckring, J. M., "Reynolds Number and Leading-Edge Bluntness Effects on a 65° Delta Wing," AIAA Paper 2002-0419, January 2002.

[10]Luckring, J. M., "Transonic Reynolds Number and Leading-Edge Bluntness Effects on a 65° Delta Wing," AIAA Paper 2003-0753, January 2003.

[11]Chu, J., and Luckring, J. M., "Experimental Surface Pressure Data Obtained on 65° Delta Wing Across Reynolds Number and Mach Number Ranges. Volume 1 – Sharp Leading Edge," NASA TM-4645, February 1996.

[12]Chu, J., and Luckring, J. M., "Experimental Surface Pressure Data Obtained on 65° Delta Wing Across Reynolds Number and Mach Number Ranges. Volume 2 – Small Leading Edge," NASA TM-4645, February 1996.

[13]Chu, J., and Luckring, J. M., "Experimental Surface Pressure Data Obtained on 65° Delta Wing Across Reynolds Number and Mach Number Ranges. Volume 3 – Medium Leading Edge," NASA TM-4645, February 1996.

[14]Chu, J., and Luckring, J. M., "Experimental Surface Pressure Data Obtained on 65° Delta Wing Across Reynolds Number and Mach Number Ranges. Volume 4 – Large Leading Edge," NASA TM-4645, February 1996.

[15]Wahls, R. A., "The National Transonic Facility – A Research Retrospective," AIAA Paper 01-0754, January 2001.

[16]Luckring, J. M., "An Overview of National Transonic Facility Investigations for High Performance Military Aerodynamics" AIAA Paper 01-0906, January 2001.

[17]Fuller, D. E., "Guide for Users of the National Transonic Facility," NASA TM-83124, 1981.

[18]Elsenaar, A., Binion, T. W. Jr., and Stanewsky, E., "Reynolds Number Effects in Transonic Flow," AGARDograph AG-303, December 1988.

[19]Abbott, I. H., and Von Doenhoff, A. E. "Theory of Wing Sections," Dover Publications, Inc., 1959.

[20]Luckring, J. M., Schoonover, W.E., Jr., and Frink, N. T. "Recent Advances in Applying Free Vortex Sheet Theory for the Estimation of Vortex Flow Aerodynamics," AIAA Paper 82-0095, January 1982.

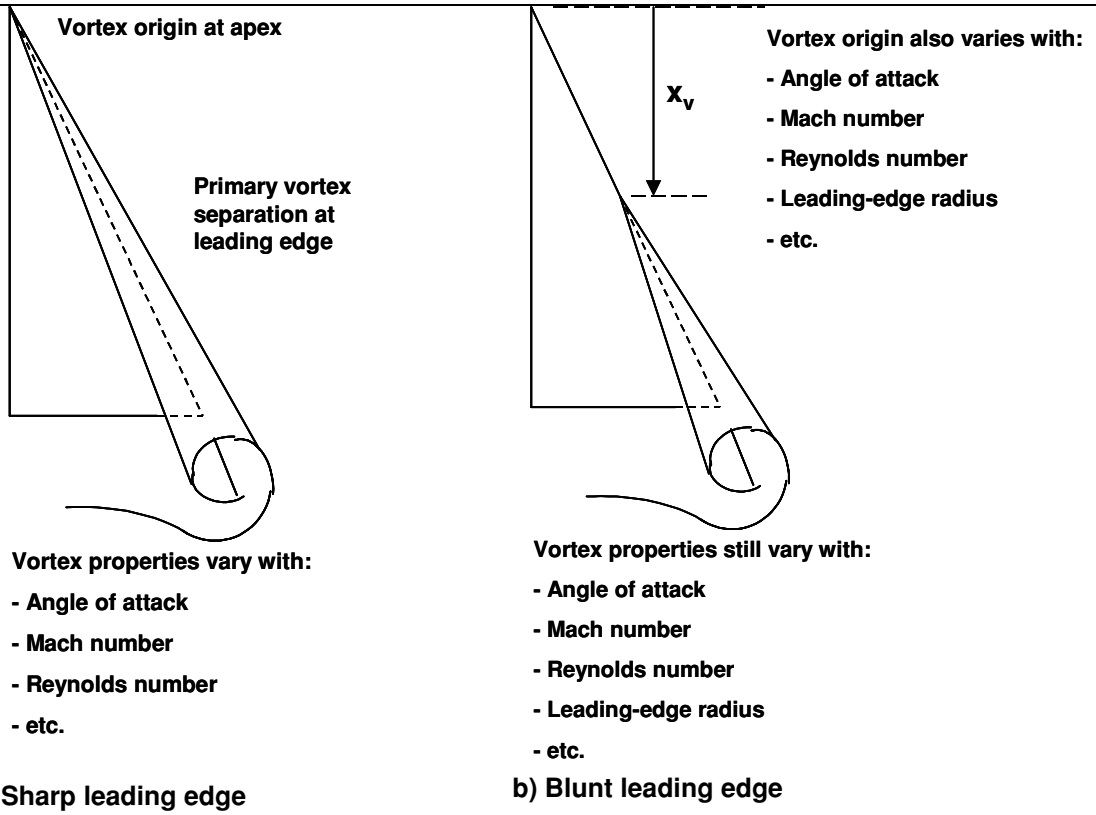

Figure 1 – Some factors affecting separation-induced leading-edge vortices.

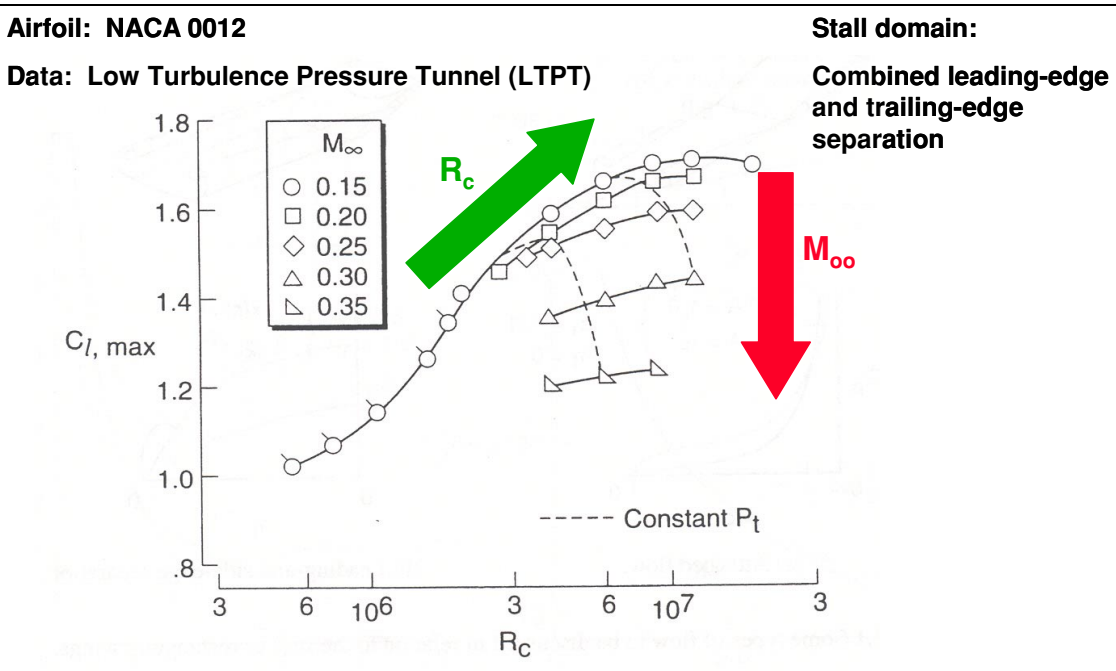

Figure 2 – Mach and Reynolds number effects on airfoil leading-edge separation (Polhamus[8]).

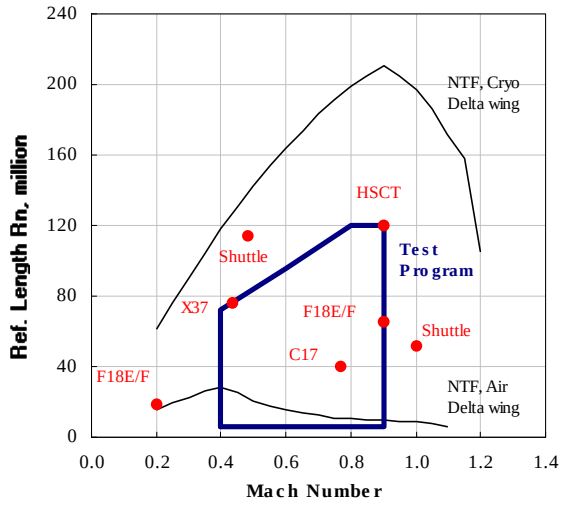

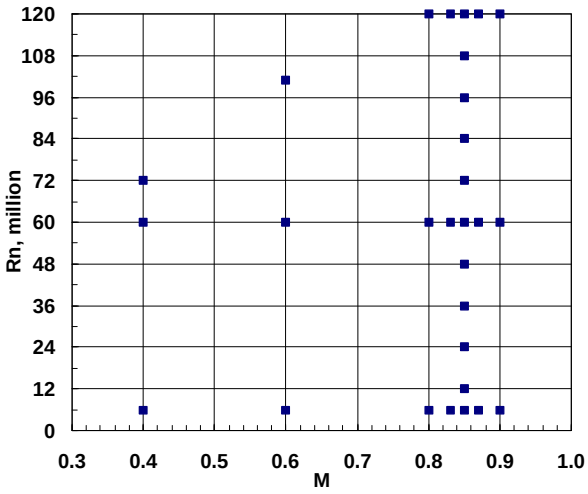

a) NTF envelopes and aircraft operating conditions.

b) Representative delta-wing test matrix.

Figure 3 – Reynolds number and Mach number conditions.

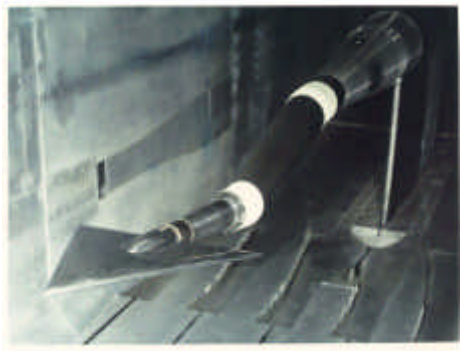

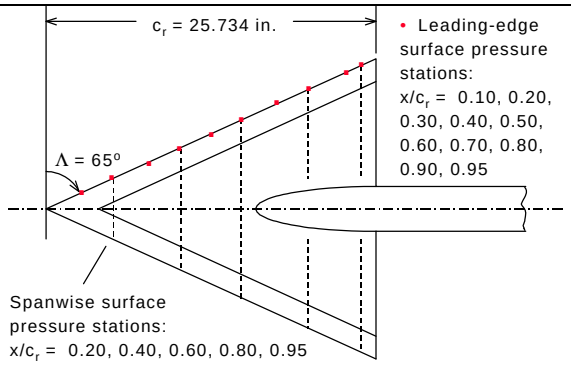

a) Model installed in NTF.

b) Instrumentation layout.

Figure 4 – NTF 65° delta wing.

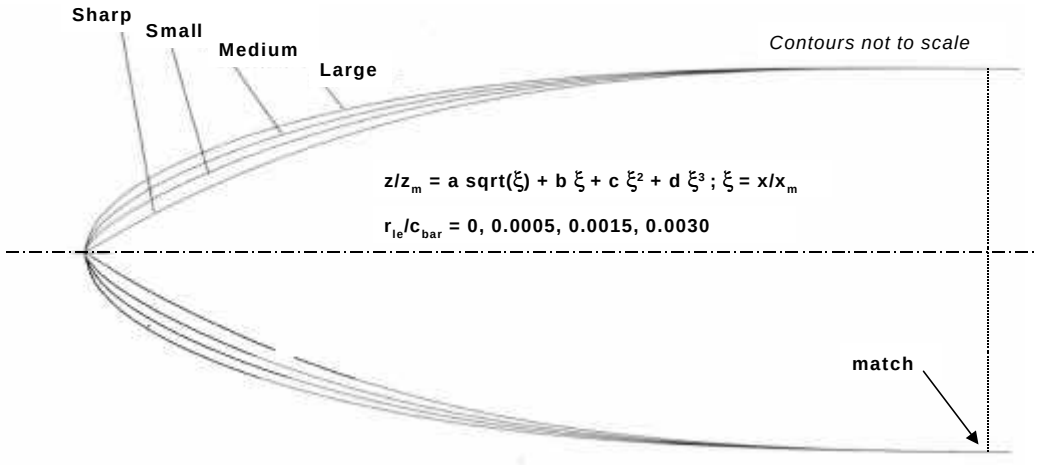

Figure 5 – Streamwise leading-edge contours for NTF delta wing.

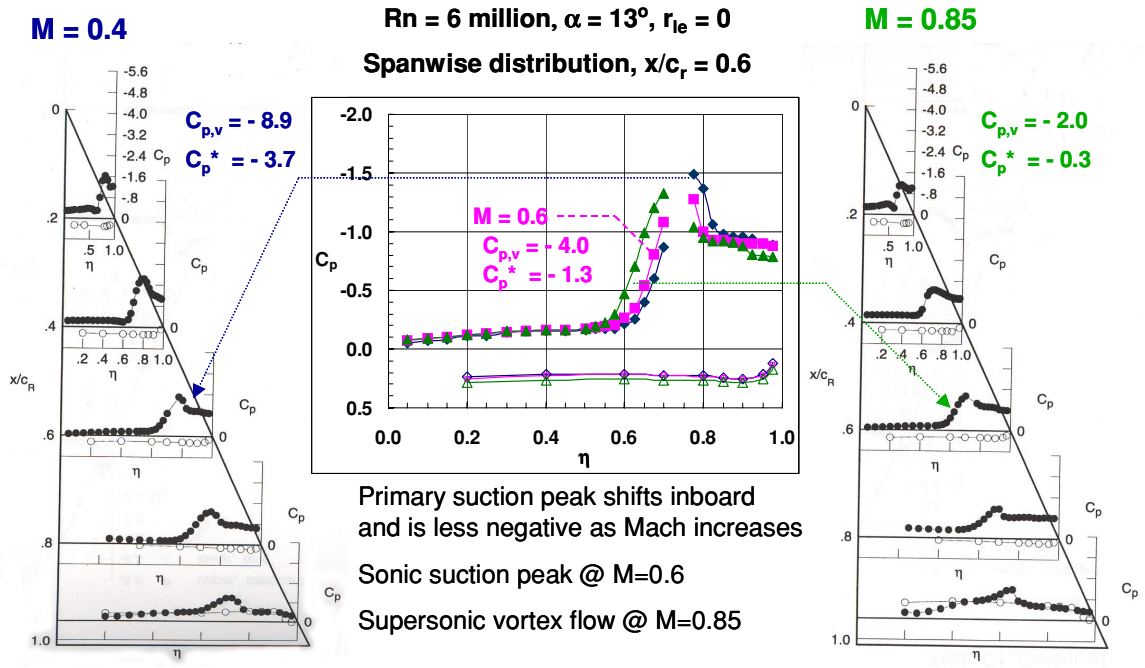

Figure 6 – Compressibility effect on sharp-edged vortex flow.

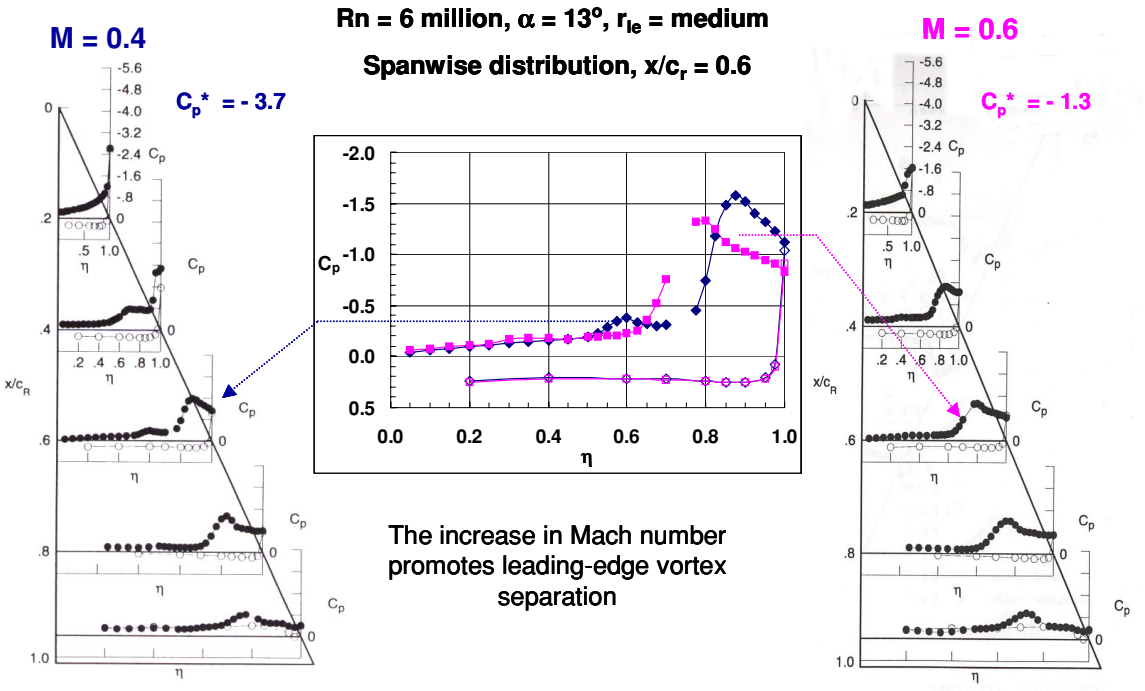

Figure 7 – Compressibility effects for a blunt-edged vortex flow.

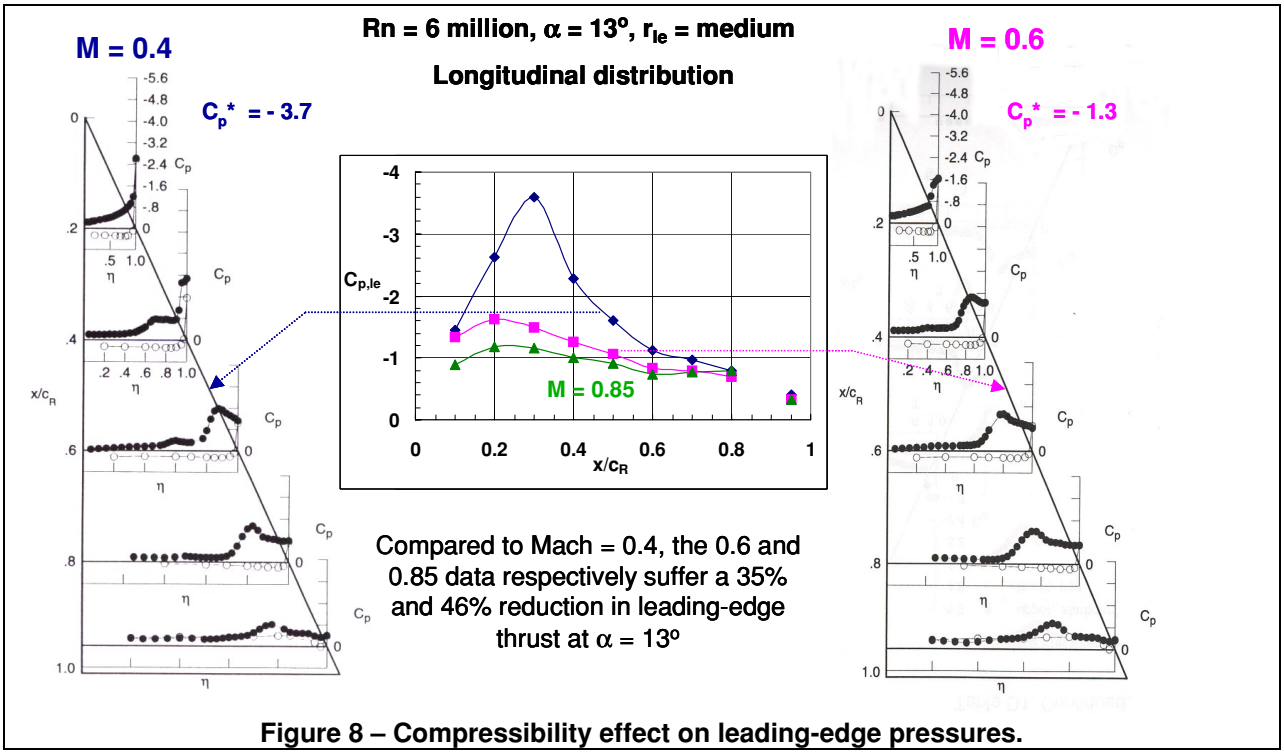

Figure 8 – Compressibility effect on leading-edge pressures.

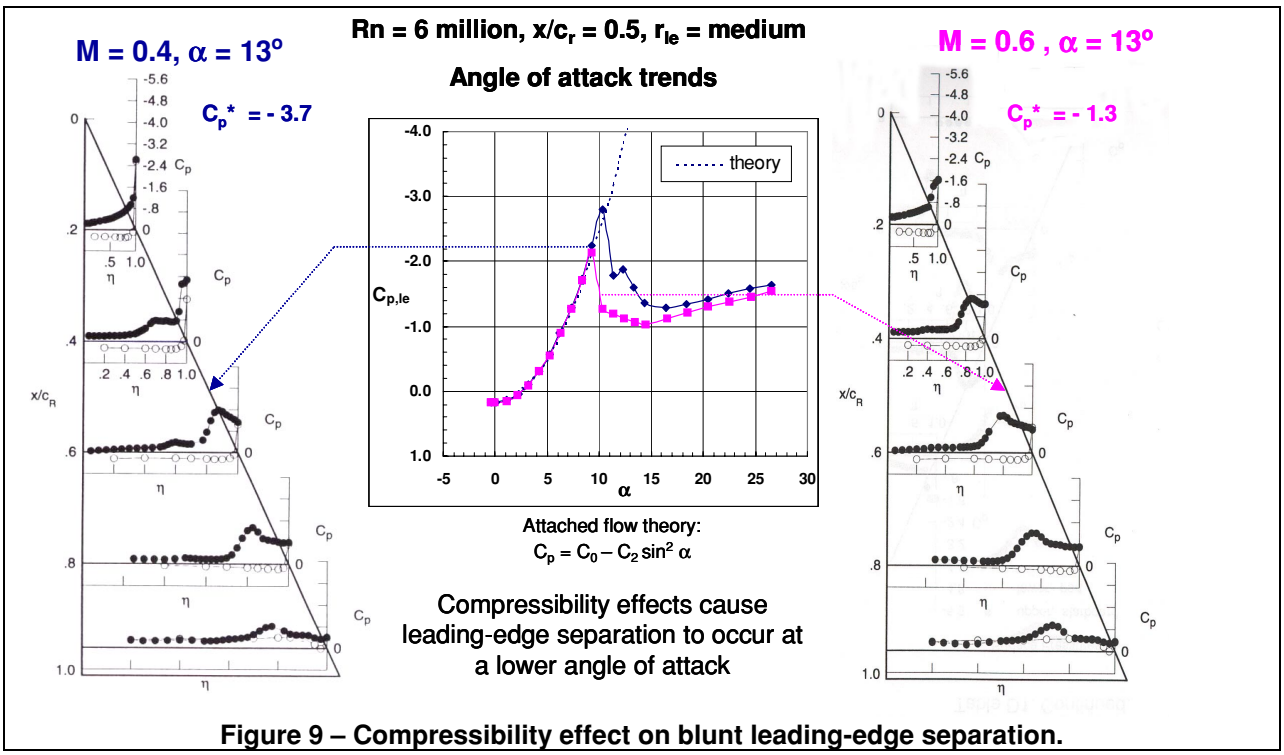

Figure 9 – Compressibility effect on blunt leading-edge separation.

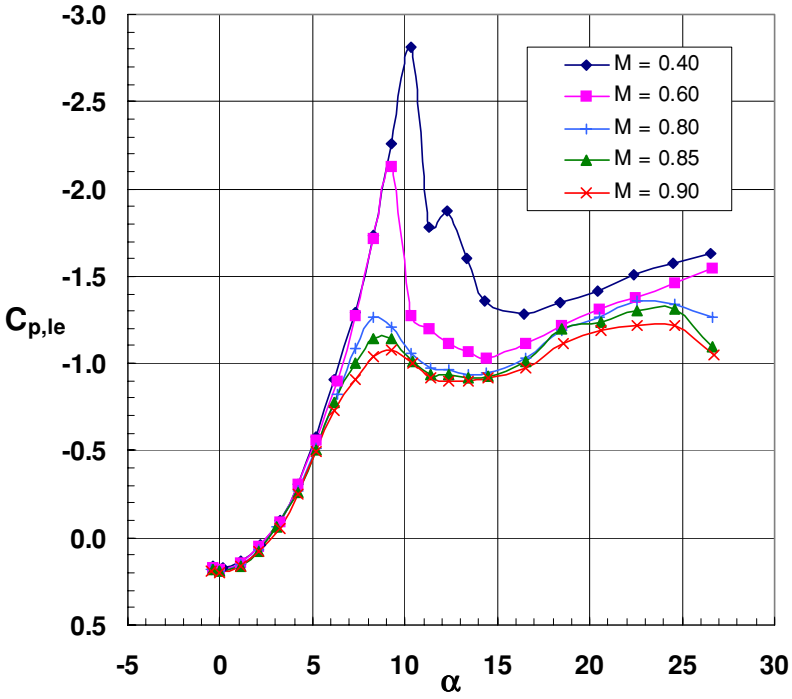

Figure 10 – Leading-edge separation characteristics for full Mach range.

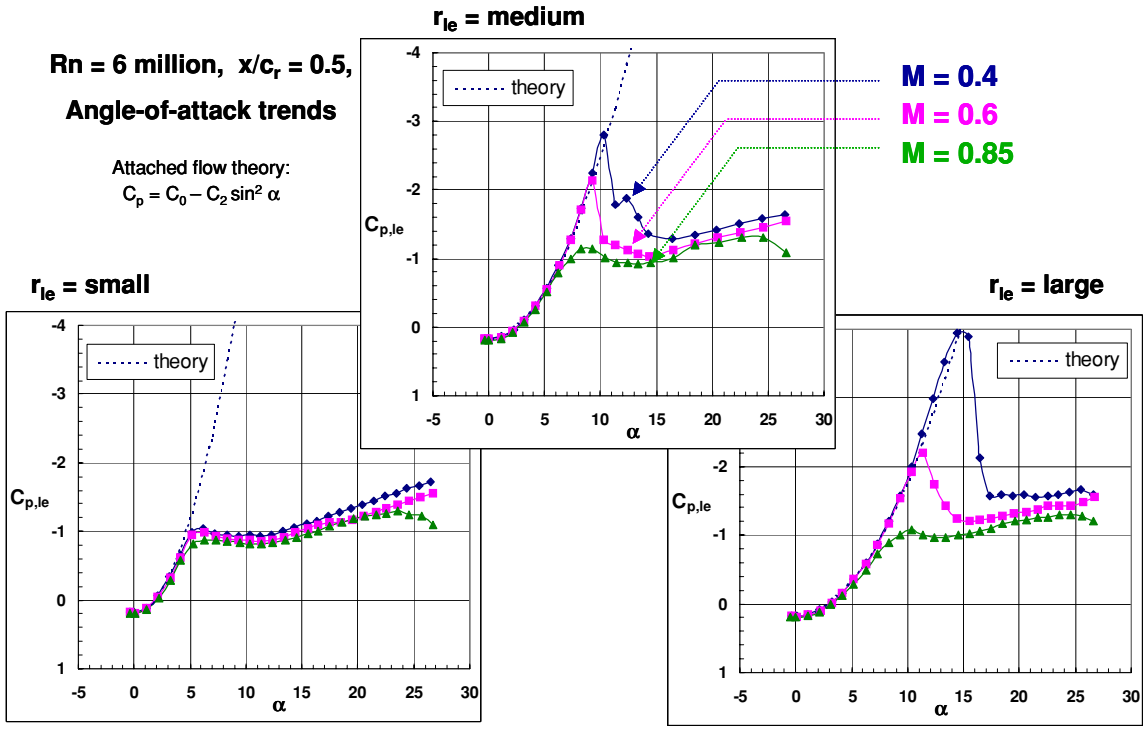

Figure 11 – Bluntness and compressibility effects for leading-edge separation.

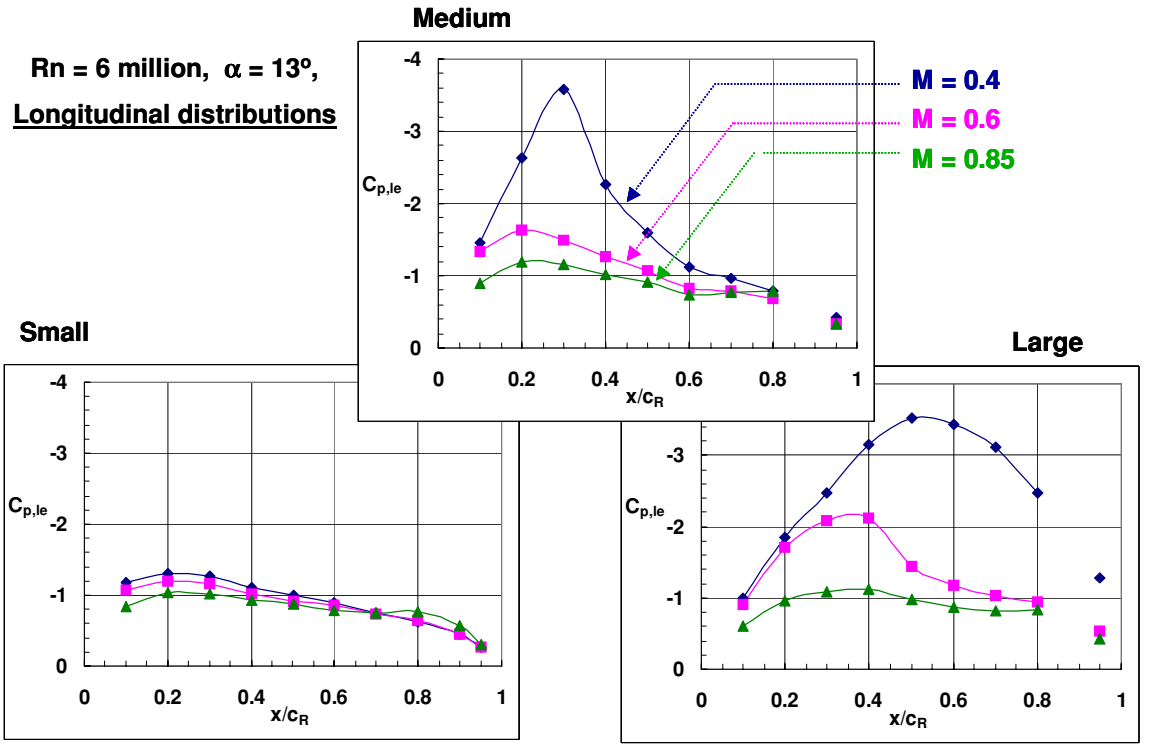

Figure 12 – Bluntness and compressibility effects on leading-edge pressure distributions.

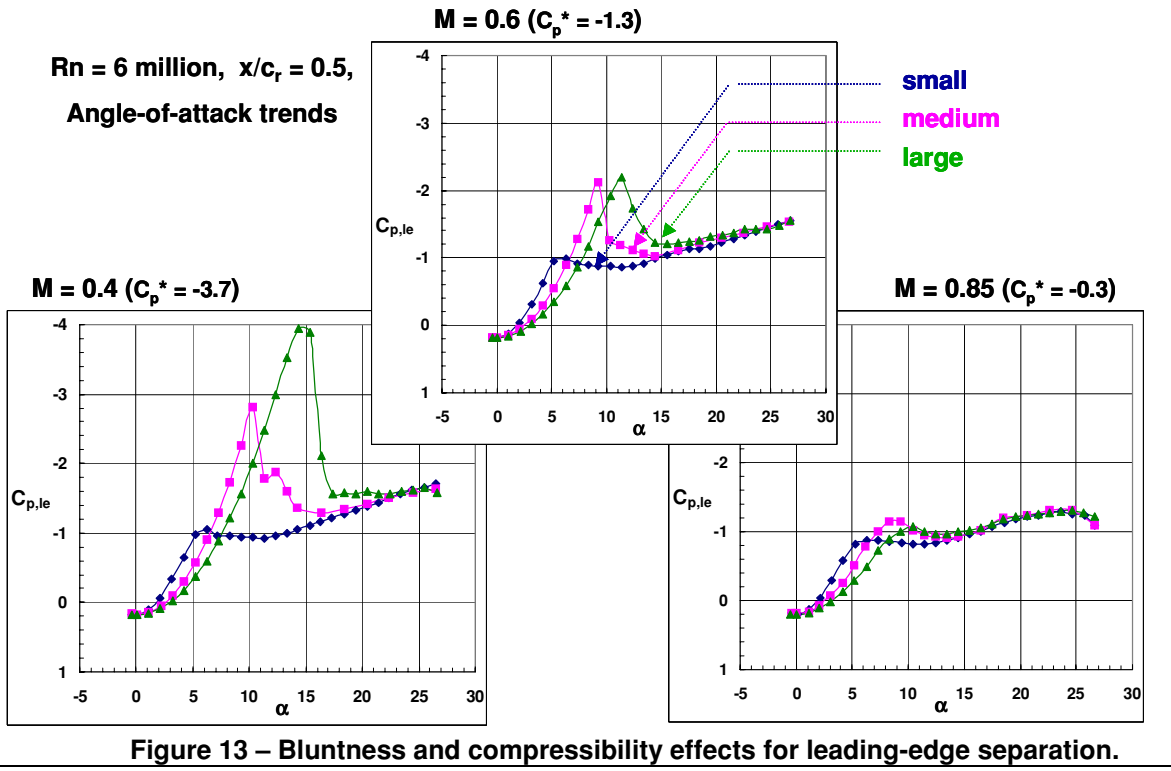

Figure 13 – Bluntness and compressibility effects for leading-edge separation.

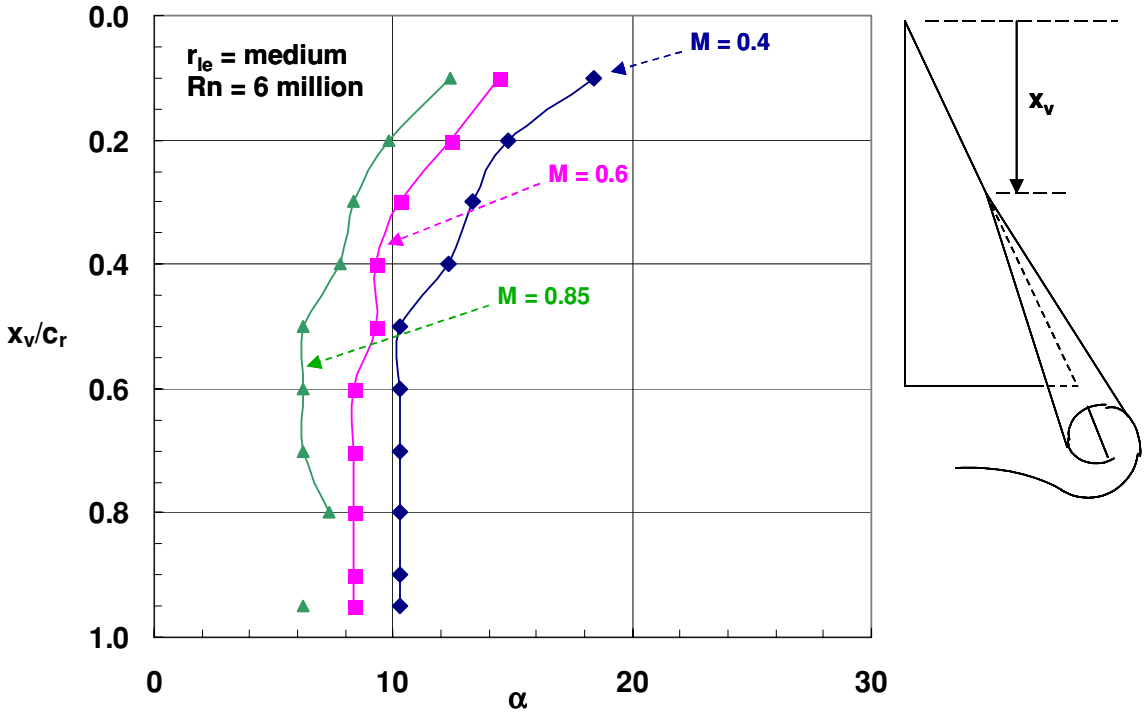

Figure 14 – Compressibility effect on leading-edge separation.

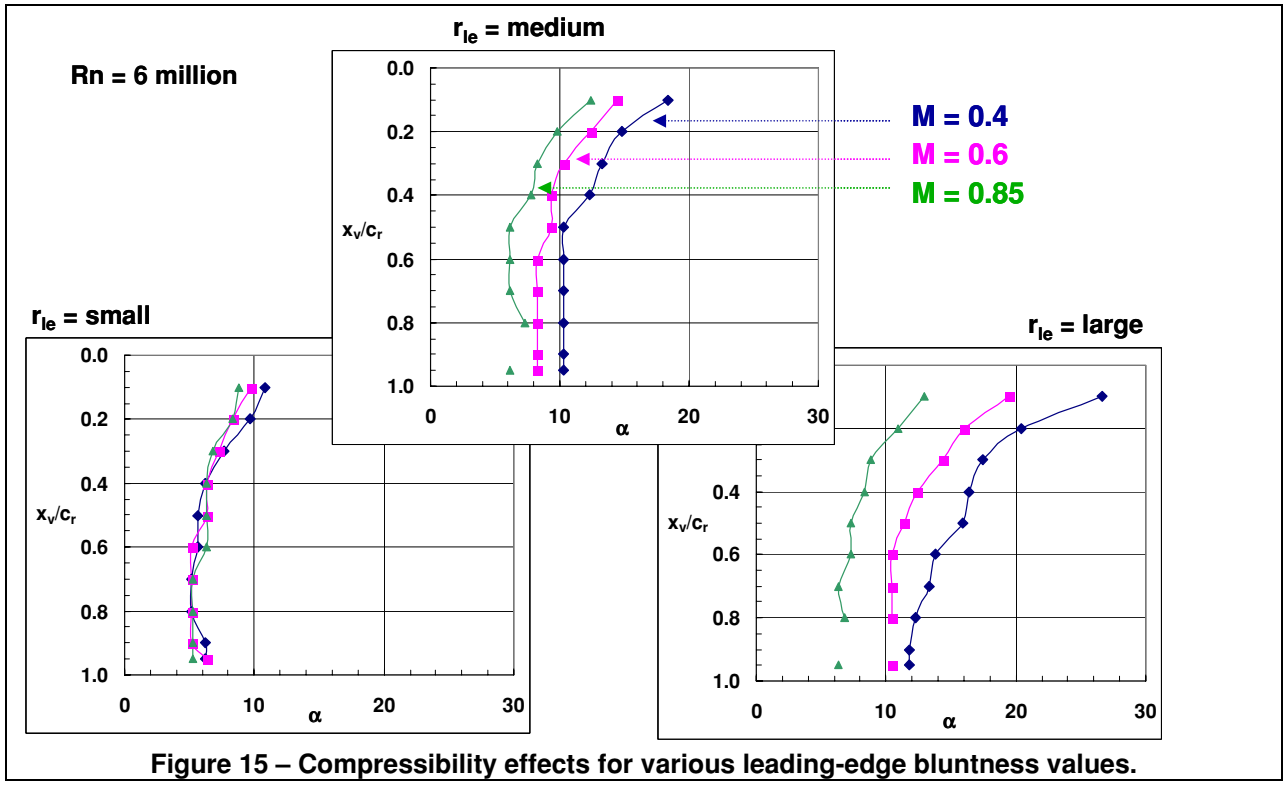

Figure 15 – Compressibility effects for various leading-edge bluntness values.

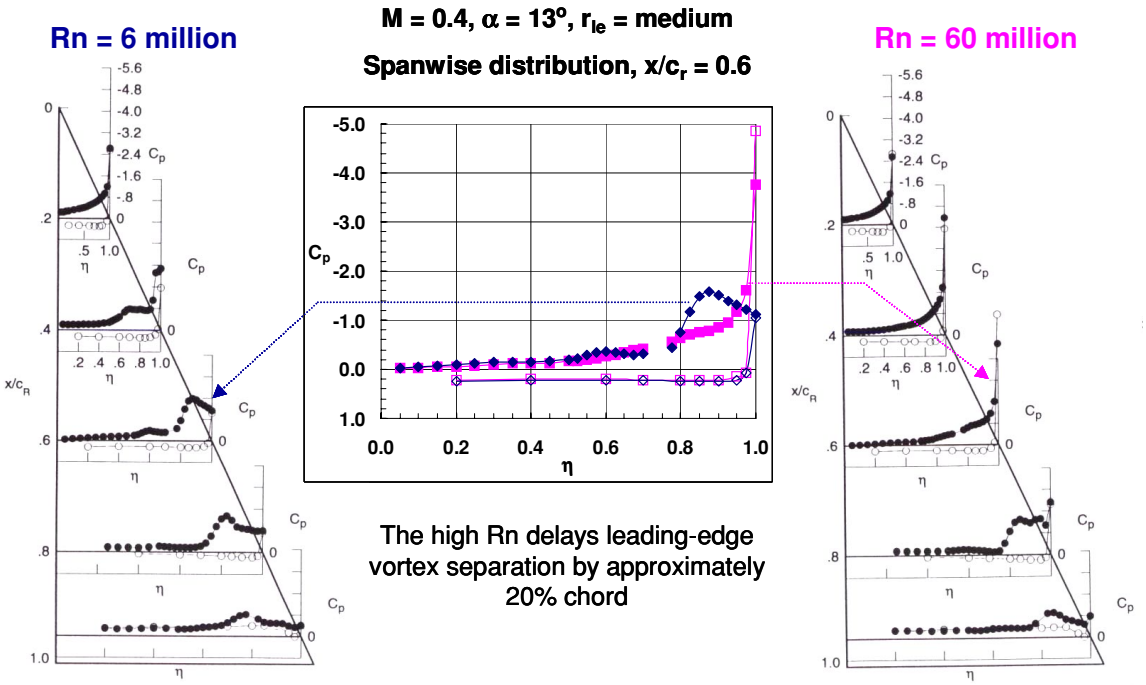

Figure 16 – Low-speed Reynolds number effect on leading-edge separation (Luckring[9]).

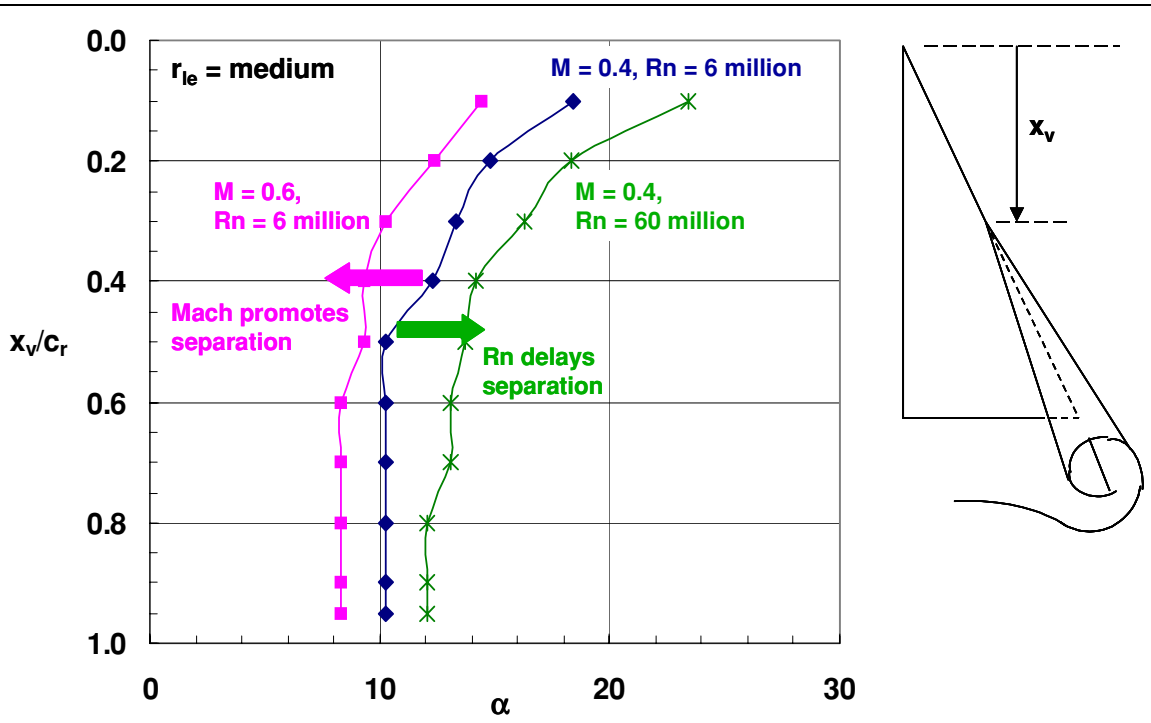

Figure 17 – Mach and Reynolds number effects on leading-edge separation.